

## Lattice dynamics and broad-band dielectric properties of the $\text{KTaO}_3$ ceramics

Sebastjan Glinšek,<sup>1,2,a)</sup> Dmitry Nuzhnyy,<sup>3</sup> Jan Petzelt,<sup>3</sup> Barbara Malič,<sup>1,2</sup> Stanislav Kamba,<sup>3</sup> Viktor Bovtun,<sup>3</sup> Martin Kempa,<sup>3</sup> Volodymyr Skoromets,<sup>3</sup> Petr Kužel,<sup>3</sup> Ivan Gregora,<sup>3</sup> and Marija Kosec<sup>1</sup>

<sup>1</sup>*Jožef Stefan Institute, Jamova cesta 39, SI-1000 Ljubljana, Slovenia*

<sup>2</sup>*Centre of Excellence SPACE-SI, Aškerčeva cesta 12, SI-1000 Ljubljana, Slovenia*

<sup>3</sup>*Institute of Physics, Academy of Sciences of the Czech Republic, Na Slovance 2, 182 21 Prague 8, Czech Republic*

(Received 4 February 2012; accepted 7 April 2012; published online 16 May 2012)

High-density  $\text{KTaO}_3$  ceramics were synthesized and studied by means of microwave, terahertz, infrared, and Raman spectroscopies. The results were analyzed together with recently published radio-frequency data. [S. Glinšek *et al.*, *J. Am. Ceram. Soc.* **94**, 1368 (2011)] Three polar modes expected for the cubic structure were observed. As in single crystals, the lowest-frequency TO1 mode (soft mode) strongly softens on cooling, while the TO2 and TO4 mode frequencies do not change with temperature. The permittivity does not show any significant dispersion below the soft mode frequency and its value in the kHz and GHz range is mainly given by the intrinsic polar lattice modes contribution. The soft mode frequency agrees with the values found in single crystals; this indicates a negligible influence of the grain boundaries on the dielectric response in  $\text{KTaO}_3$  unlike in other ferroelectric or incipient ferroelectric perovskite ceramics. © 2012 American Institute of Physics. [<http://dx.doi.org/10.1063/1.4714545>]

### I. INTRODUCTION

Incipient ferroelectrics, such as  $\text{SrTiO}_3$  and  $\text{KTaO}_3$ , exhibit increasing dielectric permittivity  $\epsilon'$  with decreasing temperature. In contrast to ferroelectrics, the ferroelectric phase does not exist at any temperature, either because the hypothetical critical temperature  $T_{cr}$  lies below 0 K or because the long-range ordering is suppressed by quantum fluctuations.<sup>1</sup> As the material approaches liquid-He temperatures, the permittivity deviates from the Curie-Weiss law and saturates according to the Barrett formula.<sup>2</sup> The compound stays in its paraelectric phase (cubic  $Pm\bar{3}m$  structure in the case of  $\text{KTaO}_3$ ) down to the lowest attainable temperatures. However, the low-temperature paraelectric state is rather unstable and the ferroelectric phase can be induced in several ways, e.g., by doping,<sup>3</sup> by uniaxial stress,<sup>4</sup> or by biaxial strain.<sup>5</sup> The last mechanism is specific for thin films, and it has received considerable attention during recent years; nevertheless, its nature is still not completely understood.<sup>6–9</sup>

The static permittivity value of incipient ferroelectrics studied to date is given exclusively by the contribution of polar optic phonons. The contribution of the lowest-frequency mode (soft mode) largely dominates; its softening (frequency decrease) upon cooling is then at the origin of the observed permittivity increase. No dielectric relaxation is observed below the soft mode frequency which lies in the THz range.<sup>10</sup> In the absence of defects, the dielectric losses in the microwave (MW) range are primarily caused by the intrinsic multiphonon absorption.<sup>11–13</sup> Owing to their high permittivity and low losses, the incipient ferroelectrics have been considered as good candidates for tunable MW applications, especially for those operating at cryogenic temperatures.

Even though  $\text{KTaO}_3$  has been extensively studied since 1960s in its single crystal form, reports on the ceramics have started to emerge only recently.<sup>14–17</sup> The main reasons for this lack of experimental data are problems encountered during the ceramic sample processing, such as hygroscopic nature of starting compounds, sublimation of potassium species upon heating, and a strongly covalent character of the Ta-O bond<sup>18</sup> which inhibits the diffusion process. It is therefore difficult to achieve the exact stoichiometry of samples, their chemical and structural homogeneity,<sup>19</sup> and their high density. Recently, good quality ceramics have been prepared by several groups.<sup>16,17</sup> They are characterized by a grain size in the micrometer range and their radio-frequency (RF) permittivity displays a low-temperature plateau with  $\epsilon' \sim 4000$ . This value is very close to that found in  $\text{KTaO}_3$  single crystals ( $\sim 4500$ ).<sup>10,20</sup>

The dielectric grain size effect was previously studied in several other high-permittivity perovskites,<sup>21</sup> most thoroughly in high-density  $\text{SrTiO}_3$  ceramics. For this compound, the low-temperature permittivity has never exceeded  $\sim 10\,000$ , which is less than one half of the averaged value of anisotropic  $\text{SrTiO}_3$  single crystals ( $\sim 25\,000$ ).<sup>22–24</sup> In fact, the value of the low-temperature permittivity of  $\text{SrTiO}_3$  ceramics strongly decreases with the decreasing grain size; e.g., the value of only 700 is reached in the case of the spark plasma sintered ceramics with the grain size of  $\sim 80$  nm. Petzelt and co-workers<sup>22,23</sup> analyzed  $\text{SrTiO}_3$  ceramics using a broad-band dielectric spectroscopy up to the far infrared (IR) range and Raman spectroscopy. They concluded that the permittivity drop with decreasing grain size is directly related to the stiffening of the soft mode frequency. Microscopically, this remarkable dielectric grain size effect, which is in fact the highest observed among high-permittivity ceramics,<sup>21</sup> was attributed to a presence of low-permittivity

<sup>a)</sup>Electronic mail: sebastjan.glinsek@ijs.si.

polar grain boundaries, which are charged due to the O-deficiency.<sup>22,23,25</sup>

The high values of  $\epsilon'$  observed in  $\text{KTaO}_3$  ceramics indicate a much smaller or negligible grain size effect. However, no broadband dielectric studies have been performed yet on  $\text{KTaO}_3$  ceramics to confirm the intrinsic origin of the observed behavior. The purpose of this work is to study the lattice dynamics of  $\text{KTaO}_3$  ceramics and compare it with single crystals. We discuss the dielectric contribution of polar phonons in comparison with the permittivity and loss values measured in the MW and RF regions in order to identify their origin in the MW and THz range.

## II. MATERIALS AND METHODS

$\text{KTaO}_3$  ceramics were prepared from mechanochemically activated stoichiometric  $\text{K}_2\text{CO}_3$ - $\text{Ta}_2\text{O}_5$  powder mixtures. A double heating at  $800^\circ\text{C}$  for 4 h was performed to obtain perovskite powders with good structural homogeneity. The powder compacts were packed in a coarse MgO powder in an alumina die and hot-pressed at  $1250^\circ\text{C}$  for 2 h. According to the XRD analysis the obtained ceramics were phase-pure perovskites. The ceramics contained 900 ppm and 71 ppm of W and Co impurities, respectively, both arising from the wear of the milling vial and balls upon high-energy milling. The density of the sintered pellets, determined by the Archimedes' method, was  $6.87\text{ g/cm}^3$ , which corresponds to a relative density of 98%. For further details on processing see Ref. 16.

Fractured surfaces of the ceramics were analyzed with a field-emission scanning electron microscope (FE-SEM) JEOL JSM-7600 F. The typical microstructure is shown in Figure 1. The grain size distribution is bimodal, with small grains situated in the regions between the large grains. The size of the small grains is ranging from  $\sim 100\text{ nm}$  to  $\sim 500\text{ nm}$ , while the larger grains can exceed  $3\text{ }\mu\text{m}$  in size.

The complex dielectric function  $\epsilon^*(\omega, T) = \epsilon'(\omega, T) - i\epsilon''(\omega, T)$  of the ceramics was measured in a broad frequency range employing several techniques. Cylindrical samples with the diameter of  $\sim 6\text{ mm}$  were mechanically polished to achieve thicknesses appropriate for individual measurements, i.e.,  $\sim 70\text{ }\mu\text{m}$  for the MW and THz transmission, and  $\sim 300\text{ }\mu\text{m}$  for the infrared reflectivity measurements.

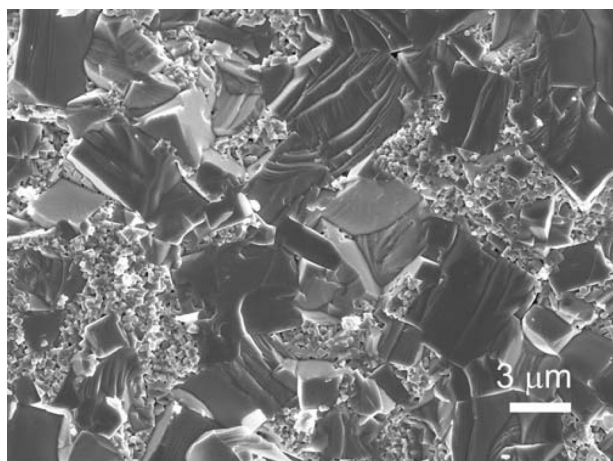


FIG. 1. FE-SEM micrograph of the fractured surface of  $\text{KTaO}_3$  ceramics.

The  $\text{TE}_{01\delta}$  dielectric resonator in the cylindrical shielding cavity was used for the MW characterization.<sup>26</sup> The dielectric permittivity and loss tangent were calculated from the resonance frequency and from the quality factor, respectively. The experiments were performed in a weakly coupled transmission setup using Agilent E8364B Network Analyzer and Janis closed-cycle He cryostat. The measurements were performed on heating from 10 K to 300 K with  $\sim 1\text{ K/min}$  heating rate. Because of the large change of the  $\text{KTaO}_3$  permittivity in the measured temperature interval, the resonant frequency changes considerably with temperature too. At room temperature, where the permittivity is rather low ( $\sim 200$ ), the frequency of resonance is found near 6 GHz, while at low temperatures, where the MW permittivity reaches nearly 4000, the resonant frequency drops to  $\sim 2\text{ GHz}$ . We stress, therefore, that the MW permittivity values were determined at the single frequency of resonance for each temperature, i.e., in the range of 2–6 GHz.

The time-domain THz transmission spectroscopy was employed for the measurements in the 100 GHz–2.5 THz ( $\sim 4$ – $80\text{ cm}^{-1}$ ) frequency range. The THz pulses were generated in an interdigitated photoconducting GaAs switch, which was illuminated by a pulse train of a femtosecond laser oscillator, and detected in a 1 mm thick [110] ZnTe crystal. A more detailed description of the experimental setup can be found in Ref. 27. The THz transmission experiment allows one to determine the complex transmission function of the sample which can be used to calculate the complex dielectric spectrum of the material as described, e.g., in Ref. 28.

The Fourier transform IR measurements were performed in a near-normal specular reflectance mode with a resolution of  $2\text{ cm}^{-1}$  using a Bruker IFS 113v spectrometer. At room temperature, the spectra were collected with pyroelectric deuterated triglycine sulfate detector in the  $25$ – $3000\text{ cm}^{-1}$  ( $0.75$ – $90\text{ THz}$ ) range, while a highly sensitive He-cooled Si bolometer detector operating at 1.5 K was used for the low-temperature measurements down to 20 K in the  $25$ – $625\text{ cm}^{-1}$  ( $0.75$ – $19\text{ THz}$ ) range.

The unpolarized Raman spectra were measured in a back-scattering configuration using Renishaw RM 1000 Raman Micro-spectrometer equipped with a grating Rayleigh filter allowing the measurement of Raman shifts down to  $\sim 20\text{ cm}^{-1}$  and with a CCD detection. The spectra were excited with a 514.5 nm line of an Ar ion laser at  $\sim 20\text{ mW}$ . The laser beam was focused to a spot of  $\sim 5\text{ }\mu\text{m}$  in diameter on the sample surface using a long-working-distance  $20\times$  microscope objective.

The low temperature measurements were performed in continuous-flow He cryostats equipped with mylar windows (THz measurements), polyethylene windows (IR), and optical windows (Raman).

## III. RESULTS AND DISCUSSION

The IR reflectivity spectrum of  $\text{KTaO}_3$  ceramics measured at room temperature is shown in Figure 2(a). For comparison, we plot also the reflectivity spectrum calculated from the measured THz transmission data. The measured



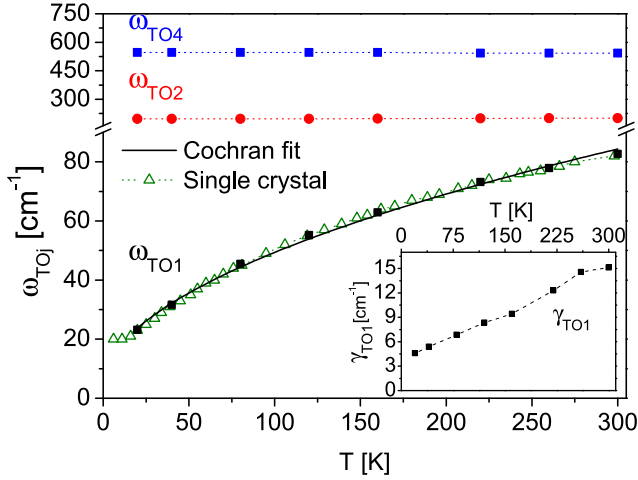


FIG. 4. Temperature dependences of the  $\omega_{TO1}$ ,  $\omega_{TO2}$ , and  $\omega_{TO4}$  polar phonon frequencies. The solid black line represents a fit of  $\omega_{TO1}$  data by the Cochran law; the dotted lines are guides to the eye. For comparison, the single crystal  $\omega_{TO1}$  data from the hyper-Raman studies are shown.<sup>32</sup> Inset: temperature dependence of the TO1 mode damping constant  $\gamma_{TO1}$ .

The resonance corresponding to the TO1 mode is the most pronounced one in the spectra and its dielectric strength strongly increases with decreasing temperature. The TO1 mode strongly softens on cooling and it obeys the Cochran law  $\omega_{TO1} \propto \sqrt{T - T_{cr}}$  in the measured temperature range. The extrapolated critical temperature can be estimated only roughly because we have only a small number of data points:  $T_{cr} = -4 \pm 2$  K; it is somewhat less than 13.1 K obtained in single crystals from the Barrett fit of the permittivity.<sup>31</sup> Indeed, the temperature dependence of  $\omega_{TO1}$  is comparable to that found in single crystals by hyper-Raman scattering.<sup>32</sup> The damping constant  $\gamma_{TO1}$  of the TO1 mode (shown in the inset of Figure 4) is also in qualitative agreement with the hyper-Raman data; it continuously decreases from the room temperature value of  $15.1 \text{ cm}^{-1}$  to  $4.6 \text{ cm}^{-1}$  at 20 K.

Ichikawa *et al.*<sup>10</sup> investigated a single crystal using time-domain THz spectroscopy; above 100 K they report slightly lower values of  $\omega_{TO1}$  and  $\gamma_{TO1}$  compared to our results and the hyper-Raman scattering data. However, in Ref. 10, the data were obtained only in a narrow frequency range below  $\omega_{TO1}$ , and we believe that within the accuracy of experiments their results correspond well to our data on ceramics.

To analyze further the polar phonons dynamics in the  $\text{KTaO}_3$  ceramics, the mode-plasma frequencies  $\Omega_{TOj}$  and the total plasma frequency  $\Omega_{TOT}$  were calculated at each measured temperature

$$\Omega_{TOj} = \sqrt{\Delta \varepsilon_j \cdot \omega_{TOj}^2}, \quad (4)$$

$$\Omega_{TOT} = \sqrt{\Omega_{TO1}^2 + \Omega_{TO2}^2 + \Omega_{TO4}^2}. \quad (5)$$

Note that the squared total plasma frequency is equal to the sum of the oscillator strengths of the polar phonon modes. In agreement with the general sum rule,  $\Omega_{TOT}$  is not temperature dependent (Figure 5). The room temperature values of the mode plasma frequencies are as follows:  $\Omega_{TO1} = 1197 \text{ cm}^{-1}$ ,  $\Omega_{TO2} = 492 \text{ cm}^{-1}$ , and  $\Omega_{TO4} = 823 \text{ cm}^{-1}$ .  $\Omega_{TO4}$  does not

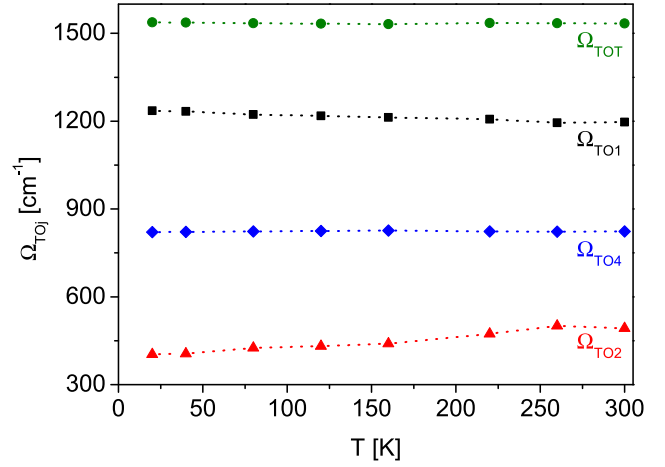


FIG. 5. Temperature dependences of the  $\Omega_{TO1}$ ,  $\Omega_{TO2}$ , and  $\Omega_{TO4}$  mode-plasma frequencies, together with the total plasma frequency  $\Omega_{TOT}$ . Lines between the points are guides to the eye.

change with temperature, while  $\Omega_{TO1}$  and  $\Omega_{TO2}$  show slight temperature dependences:  $\Omega_{TO1} = 1236 \text{ cm}^{-1}$  and  $\Omega_{TO2} = 403 \text{ cm}^{-1}$  at 20 K. These dependences indicate a rather small but detectable coupling of the two low-frequency modes.

The mode-plasma frequencies are proportional to the effective charges of the modes and may be used for an assignment of the dielectric response function to the atomic displacements in the crystal lattice. A comparison of the  $\Omega_{TOj}$  values of the  $\text{KTaO}_3$  ceramics to the literature data on typical cubic  $\text{ABO}_3$  perovskites<sup>33</sup> yields that the TO1 mode primarily corresponds to the vibration of  $\text{Ta}^{5+}$  ions against rigid  $\text{O}_6$  octahedra (Slater mode). The TO2 mode is mainly related to the vibration of  $\text{K}^+$  ions against a rigid  $\text{TaO}_6$  structure (Last mode), while the TO4 mode corresponds to a bending of the  $\text{O}_6$  octahedra (Axe mode). The result is also in agreement with the theoretical calculations.<sup>34</sup>

Temperature dependence of  $\varepsilon'$  at 1 kHz (Figure 6) has been fitted by the Barrett formula<sup>2</sup>

$$\varepsilon' = \varepsilon_b + \frac{C}{\frac{T_1}{2} \cdot \coth \frac{T_1}{2T} - T_{cr}}, \quad (6)$$

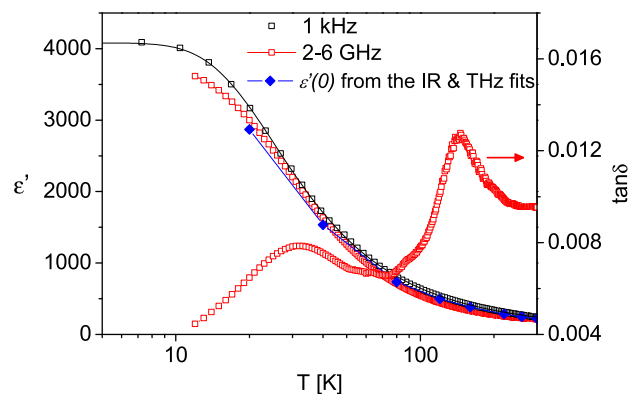


FIG. 6. Temperature dependence of the RF (1 kHz) and MW (2–6 GHz) dielectric permittivity  $\varepsilon'$  compared to the phonon contribution calculated from the IR and THz data. The microwave loss tangent is also shown. The 1 kHz measurement is taken from Ref. 16, and the line between the experimental points is a fit with the Barrett law. Other lines are guides to the eye.

and the obtained values of the fit parameters are as follows:  $C = 51\,000\text{ K}$ ,  $T_l = 56\text{ K}$ ,  $T_{cr} = 15\text{ K}$ , and  $\varepsilon_b = 64$ . They correspond well to those previously reported for single crystals<sup>31,35</sup> (a slightly lower value of  $C$  is found in our ceramic samples). The phonon contribution to the permittivity  $\varepsilon'(0)$  obtained from the IR and THz fits is in a good agreement with the MW permittivity values and also with the RF data published in Ref. 16 (see Figure 6). The small differences at low temperatures are within the accuracy of the MW experiment and of the IR fit. Slightly different microstructures of individual samples can also contribute to this difference. The results show that the low frequency permittivity in  $\text{KTaO}_3$  ceramics is mainly of intrinsic origin, i.e., arising from the polar phonons contribution.

The loss tangent in the MW range attains the values  $9.5 \times 10^{-3}$  and  $5.2 \times 10^{-3}$  at 300 and 20 K, respectively (see Figure 6). These values are higher than in single crystals where one finds for 3 GHz:  $1.4 \times 10^{-4}$  and  $4.2 \times 10^{-5}$  at 300 and 5.4 K, respectively.<sup>12</sup> Two loss peaks are observed at  $\sim 145$  and 32 K. Assuming an Arrhenius-type temperature dependence of the relaxation frequency the first peak corresponds to the relaxation observed in  $\text{KTaO}_3$  ceramics<sup>16</sup> and single crystals<sup>3</sup> near 45 K at 1 kHz. Its origin remains unclear, but apparently it is related to lattice defects and/or impurities.<sup>3</sup> The second maximum in the MW loss-spectrum (32 K) lies in the same temperature range as that reported previously for single crystals.<sup>36,37</sup> It was ascribed to the interaction between the transverse optic and longitudinal acoustic modes, partially driven by defects.<sup>36,37</sup>

The observed temperature dependences of the broadband permittivity and soft mode frequency in the  $\text{KTaO}_3$  ceramics are typical for incipient ferroelectrics. Their values are comparable to those of single crystal; this indicates rather small influence of grain boundaries on the macroscopic dielectric response. However, higher MW losses and their temperature dependence indicate presence of some defects in the ceramics.

Raman spectra of the ceramics measured at selected temperatures are presented in Figure 7. At higher temperatures, the spectra are dominated by the second-order features with broad room temperature maxima at  $119\text{ cm}^{-1}$ ,  $159\text{ cm}^{-1}$ ,  $280\text{ cm}^{-1}$ ,  $461\text{ cm}^{-1}$ ,  $584\text{ cm}^{-1}$ ,  $691\text{ cm}^{-1}$ , and  $746\text{ cm}^{-1}$ , which are in a good agreement with the single crystal data.<sup>38</sup> At temperatures below  $\sim 150\text{ K}$  sharp bands, corresponding to the IR active modes, start to emerge and their intensity increases with decreasing temperature. Similar Raman-forbidden first-order scattering was observed at low temperatures also in the “nominally pure”  $\text{KTaO}_3$  single crystals. It was ascribed to the local polar nanoregions which can be either dynamic—in this case they could be of intrinsic (anharmonic) origin—or static, induced by some unavoidable symmetry-breaking defects.<sup>39,40</sup> The cluster dynamics is usually relaxational, and it appears as a so called central peak in the microwave spectra. No such feature was observed in our experiments. We can thus conclude that the most plausible origin of the first order Raman scattering would be defects due to the presence of Co (and W) detected by the chemical analysis,<sup>16</sup> and a possible slight off-stoichiometry.

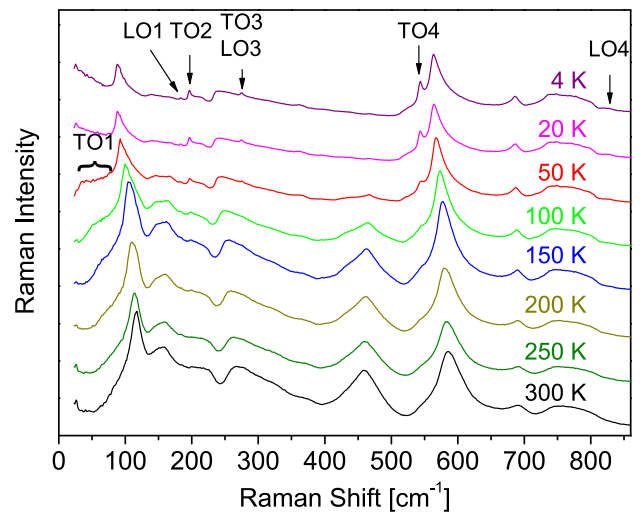


FIG. 7. Raman spectra of  $\text{KTaO}_3$  ceramics measured at selected temperatures. The spectra are displaced vertically for clarity. The positions of the Raman-forbidden one phonon features are marked.

The details of the fitting procedure of the Raman spectrum measured at 50 K are presented in Figure 8. The spectra were fitted in the range from  $22\text{ cm}^{-1}$  to  $860\text{ cm}^{-1}$  by a sum of harmonic oscillators multiplied by the corresponding Stokes temperature factor. The Rayleigh scattering tail at low frequencies was modeled by a temperature independent zero-centered mixed Gaussian-Lorentzian peak with a fixed width. The same function was used also for the artifact laser plasma peak at  $\sim 26\text{ cm}^{-1}$ . The harmonic oscillators used for the fits of the second-order features do not have a straightforward physical interpretation. They just represent a phenomenological description of the broad background scattering. The frequencies of the one-phonon modes at selected temperatures are collected and compared to those obtained from the IR and THz fits as well as from hyper-Raman data on single crystals in Table I. The frequency of the TO1 mode decreases with decreasing temperature and falls beyond our spectral range below 20 K. The rest of the modes do not show a significant temperature dependence, and their

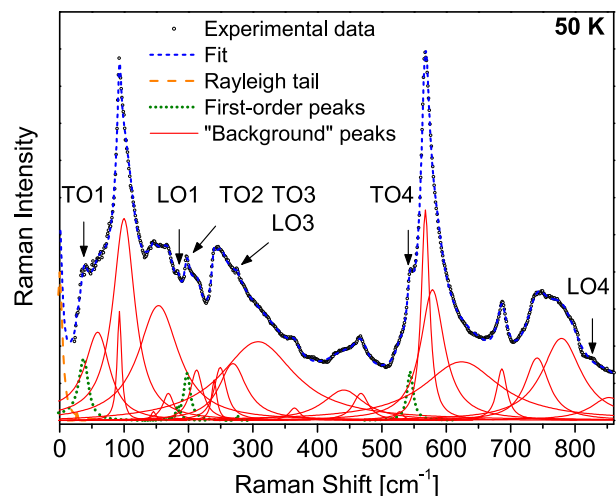


FIG. 8. Fit of the Raman spectrum measured at 50 K. Positions of one phonon peaks are marked.

TABLE I. Phonon mode frequencies (in  $\text{cm}^{-1}$ ) of  $\text{KTaO}_3$  ceramics obtained by the Raman and IR spectroscopies at selected temperatures. For comparison, room temperature single crystal values (SC), obtained from the hyper-Raman measurements, are added.<sup>35</sup>

Phonon Mode	20 K		50 K Raman	40 K IR	150 K Raman	160 K IR	300 K	
	Raman	IR					IR	SC
TO1	—	23	39	32	66	63	83	81
LO1	184	185	182	185	—	186	187	185
TO2	197	196	198	196	203	198	201	199
TO3 (LO3)	274	—	275	—	—	—	—	279
LO2 <sup>a</sup>	—	420	—	420	—	420	422	422
TO4	544	546	544	546	547	546	543	546
LO4	828	825	828	825	—	825	825	826

<sup>a</sup>Since TO3 (LO3) mode is IR-inactive, this mode is denoted as the LO2, which differs from Ref. 35, where it is denoted as the LO3 mode.

frequencies are in a good agreement with the room temperature values for the single crystals.<sup>35</sup>

Further investigations of smaller grain size ceramics by means of high-resolution transmission electron microscopy and broad-band dielectric spectroscopy are needed in order to estimate the possible dielectric grain size effect in  $\text{KTaO}_3$  ceramics: identify the type of the majority of defects, their spatial position, and the structure of grain boundaries.

#### IV. CONCLUSIONS

$\text{KTaO}_3$  ceramics with a 98% relative density were synthesized; their microstructure is bimodal with grain sizes of a few hundreds of nanometers and several micrometers. The samples were characterized by a number of spectroscopic techniques in a broad spectral range. The three polar optic phonons, TO1 (Slater mode), TO2 (Last mode), and TO4 (Axe mode), known from single crystals, were observed by the THz and infrared spectroscopies, and a weak coupling of the Slater and Last modes was revealed by the mode-plasma frequencies analysis. On the one hand, higher MW losses (compared to single crystals), their temperature dependence and the presence of first-order Raman spectra indicate an existence of defects in the  $\text{KTaO}_3$  ceramics. On the other hand, the high value of the low-temperature permittivity and the strong softening of the TO1 mode (both characteristics in agreement with those found in single crystals) show a negligible influence of grain boundaries on the macroscopic dielectric response of the ceramics.

#### ACKNOWLEDGMENTS

This work was financially supported by Slovenian Research Agency (Program No. P2-0105; young researcher program, Contract No. 10000-07-3100068), European Cooperation in Science and Technology (STSM in the frame of COST Action MP0904), by the European Union, by Ministry of Higher Education, Science and Technology of Slovenia, the Czech Science Foundation (Project Nos. P204/12/0232 and 202/09/H041) and the Grant Agency of the Charles University (Project No. SVV-2012-265303).

- <sup>1</sup>K. A. Müller and H. Burkard, *Phys. Rev. B* **19**, 3593 (1979).
- <sup>2</sup>J. H. Barrett, *Phys. Rev.* **86**, 118 (1952).
- <sup>3</sup>G. A. Samara, *J. Phys.: Condens. Matter* **15**, R367 (2003).
- <sup>4</sup>H. Uwe and T. Sakudo, *Phys. Rev. B* **13**, 271 (1976).
- <sup>5</sup>D. Nuzhnyy, J. Petzelt, S. Kamba, P. Kužel, C. Kadlec, V. Bovtun, M. Kempa, J. Schubert, C. M. Brooks, and D. G. Schlom, *Appl. Phys. Lett.* **95**, 232902 (2009).
- <sup>6</sup>J. H. Haeni, P. Irvin, W. Chang, R. Uecker, P. Reiche, Y. L. Li, S. Choudhury, W. Tian, M. E. Hawley, B. Craigo, A. K. Tagantsev, X. Q. Pan, S. K. Streiffer, L. Q. Chen, S. W. Kirchoefer, J. Levy, and D. G. Schlom, *Nature* **430**, 758 (2004).
- <sup>7</sup>M. Tyunina, J. Narkilahti, M. Plekh, R. Oja, R. M. Nieminen, A. Dejneka, and V. Trepakov, *Phys. Rev. Lett.* **104**, 227601 (2010).
- <sup>8</sup>V. Skoromets, S. Glinšek, V. Bovtun, M. Kempa, J. Petzelt, S. Kamba, B. Malič, M. Kosec, and P. Kužel, *Appl. Phys. Lett.* **99**, 052908 (2011).
- <sup>9</sup>Y. S. Kim, J. S. Choi, J. Kim, S. J. Moon, B. H. Park, J. Yu, J. H. Kwon, M. Kim, J. S. Chung, T. W. Noh, and J. G. Yoon, *Appl. Phys. Lett.* **97**, 242907 (2010).
- <sup>10</sup>Y. Ichikawa, M. Nagai, and K. Tanaka, *Phys. Rev. B* **71**, 092106 (2005).
- <sup>11</sup>A. K. Tagantsev, V. O. Sherman, K. F. Astafiev, J. Venkatesh, and N. Setter, *J. Electroceram.* **11**, 5 (2003).
- <sup>12</sup>R. G. Geyer, B. Riddle, J. Krupka, and L. A. Boatner, *J. Appl. Phys.* **97**, 104111 (2005).
- <sup>13</sup>S. Kamba, M. Savinov, F. Laufek, O. Tkáč, C. Kadlec, S. Veljko, E. J. John, G. Subodh, M. T. Sebastian, M. Klementová, V. Bovtun, J. Pokorný, V. Goian, and J. Petzelt, *Chem. Mater.* **21**, 811 (2009).
- <sup>14</sup>Z. X. Chen, X. L. Zhang, and L. E. Cross, *J. Am. Ceram. Soc.* **66**, 511 (1983).
- <sup>15</sup>A. K. Axelsson, Y. Pan, M. Valant, and N. Alford, *J. Am. Ceram. Soc.* **92**, 1773 (2009).
- <sup>16</sup>S. Glinšek, B. Malič, T. Rojac, C. Filipič, B. Budič, and M. Kosec, *J. Am. Ceram. Soc.* **94**, 1368 (2011).
- <sup>17</sup>A. Tkach, P. M. Vilarinho, and A. Almeida, *J. Eur. Ceram. Soc.* **31**, 2303 (2011).
- <sup>18</sup>A. Villesuzanne, C. Elissalde, M. Pouchard, and J. Ravez, *Eur. Phys. J. B* **6**, 307 (1998).
- <sup>19</sup>E. Tchernykhova, S. Glinšek, B. Malič, and M. Kosec, *J. Am. Ceram. Soc.* **94**, 1611 (2011).
- <sup>20</sup>B. Salce, J. L. Gravi, and L. A. Boatner, *J. Phys.: Condens. Matter* **6**, 4077 (1994).
- <sup>21</sup>J. Petzelt, *Ferroelectrics* **400**, 117 (2010).
- <sup>22</sup>J. Petzelt, T. Ostapchuk, I. Gregora, D. Nuzhnyy, I. Rychetsky, K. Maca, and Z. Shen, *Ferroelectrics* **363**, 227 (2008).
- <sup>23</sup>J. Petzelt, T. Ostapchuk, I. Gregora, I. Rychetsky, S. Hoffmann-Eifert, A. V. Pronin, Y. Yuzyuk, B. P. Gorshunov, S. Kamba, V. Bovtun, J. Pokorný, M. Savinov, V. Porokhonsky, D. Rafaja, P. Vaněk, A. Almeida, M. R. Chaves, A. A. Volkov, M. Dressel, and R. Waser, *Phys. Rev. B* **64**, 184111 (2001).
- <sup>24</sup>T. Sakudo and H. Unoki, *Phys. Rev. Lett.* **26**, 851 (1971).
- <sup>25</sup>J. Petzelt, T. Ostapchuk, I. Gregora, P. Kuzel, J. Liu, and Z. Shen, *J. Phys.: Condens. Matter* **19**, 196222 (2007).
- <sup>26</sup>J. Krupka, K. Derzakowski, B. Riddle, and J. Baker-Jarvis, *Meas. Sci. Technol.* **9**, 1751 (1998).
- <sup>27</sup>P. Kužel, H. Nemeč, F. Kadlec, and C. Kadlec, *Opt. Express* **18**, 15338 (2010).
- <sup>28</sup>P. Kuzel and J. Petzelt, *Ferroelectrics* **239**, 79 (2000).
- <sup>29</sup>R. C. Miller and W. G. Spitzer, *Phys. Rev.* **129**, 94 (1963).
- <sup>30</sup>C. H. Perry and T. F. McNelly, *Phys. Rev.* **154**, 456 (1967).
- <sup>31</sup>G. A. Samara and B. Morosin, *Phys. Rev. B* **8**, 1256 (1973).
- <sup>32</sup>H. Vogt, *Phys. Rev. B* **51**, 8046 (1995).
- <sup>33</sup>J. Hlinka, J. Petzelt, S. Kamba, D. Nuzhnyy, and T. Ostapchuk, *Phase Transitions* **79**, 41 (2006).
- <sup>34</sup>D. J. Singh, *Phys. Rev. B* **53**, 176 (1996).
- <sup>35</sup>H. Vogt and H. Uwe, *Phys. Rev. B* **29**, 1030 (1984).
- <sup>36</sup>I. M. Buzin, I. V. Ivanov, and V. A. Chistyakov, *Fiz. Tverd. Tela* **9**, 2 (1980).
- <sup>37</sup>V. Belokopytov, I. V. Ivanov, S. I. Katanov, N. N. Moiseev, and P. P. Symikov, *Fiz. Tverd. Tela* **24**, 3 (1982).
- <sup>38</sup>W. G. Nilsen and J. G. Skinner, *J. Chem. Phys.* **47**, 1413 (1967).
- <sup>39</sup>H. Uwe, K. B. Lyons, H. L. Carter, and P. A. Fleury, *Phys. Rev. B* **33**, 6436 (1986).
- <sup>40</sup>H. Vogt, *J. Phys.: Condens. Matter* **3**, 3697 (1991).